Transmitter and Receiver Motion Constraints for Bistatic Synthetic Aperture Sonar

T.J. Sutton and H.D. Griffiths
Dept of Electronic & Electrical Engineering
University College London
Torrington Place
London WC1E 7JE
United Kingdom

t.sutton@ee.ucl.ac.uk; h.griffiths@ee.ucl.ac.uk

ABSTRACT

A bistatic synthetic aperture sonar (SAS) mounted on an AUV offers many promising advantages over a conventional monostatic SAS system. As the transmitter is supported remotely from the AUV, there are substantial weight, cost and power savings when designing an AUV to carry only the receiver hydrophone array and processing electronics. In addition, bistatic SAS images will have two shadows (one each for the transmitter and receiver), potentially aiding the process of target classification. Many mine targets are designed to have a low signature for monostatic sonar transmissions, and a further advantage of bistatic SAS is its use of the sound field that is scattered away from the direction of the transmitter.

The paper sets out the constraints on the motion of the transmitter and the receiver hydrophone array if the returning signal from the target area is to be adequately spatially sampled. In particular, it is shown that the movement of the transmitter is severely constrained if a chosen target area is to be imaged without grating lobes, while under favourable circumstances the receiver array can move its entire length between pings (rather than half its length as in the case of monostatic SAS).

1.0 INTRODUCTION

A near-term goal in Mine Countermeasure (MCM) operations is the deployment of small autonomous underwater vehicles (AUVs) that use sidescan sonar imaging or synthetic aperture sonar to image the seabed at high resolution, identify candidate mine-like objects, and classify them automatically in real time using sophisticated on-board software.

The problem of detecting and classifying mines automatically and reliably is exceedingly difficult. The seabed varies greatly from place to place in its texture and reflectivity. In addition the seabed texture is likely to be punctuated by rocks or debris, which create shadows in the sonar image and appear mine-like. The mines themselves may be designed to have a low scattering cross-section for sound, and they may be partly or completely buried by the action of ocean currents. In this situation there is no single reliable technique to distinguish mines from other objects on the seabed.

Bistatic sonar techniques offer some significant attractions:

(1) Improved detection against ‘stealthy’ targets (such as the Swedish ROCKAN mine) which are shaped to reduce the monostatic signature.

Sutton, T.J.; Griffiths, H.D. (2006) Transmitter and Receiver Motion Constraints for Bistatic Synthetic Aperture Sonar. In *Bistatic-Multistatic Radar and Sonar Systems* (pp. 16-1 – 16-12). Meeting Proceedings RTO-MP-SET-095, Paper 16. Neuilly-sur-Seine, France: RTO. Available from: http://www.rto.nato.int/abstracts.asp.

(2) Use with a stand-off co-operative source would permit a simple receive-only system on an AUV (or multiple AUVs), which could image a target from a variety of geometries, which would avoid the power requirements of a transmitter and which would be totally passive. This could provide a simple and effective adjunct to the existing MCM capability, and a step on the way to a fully AUV-based capability.

(3) A geometry in which the target scene is insonified from a distance but with a bistatic receiver looking downwards at high incidence angle may be effective against buried mines, since the target-to-receiver path is through a sediment layer of minimum thickness.

(4) A bistatic imaging geometry gives two shadows of a target – one from the transmitter and one from the receiver (this has recently been demonstrated by QinetiQ Malvern in airborne bistatic SAR imagery [1]). Having two shadows immediately provides twice the amount of information, from a single image, giving the potential for significantly better target shape information.

However, the bistatic geometry does introduce additional complications in terms of timing and location of the transmitter and receiver systems.

Initial studies of bistatic sonar have looked particularly at the problem of identifying buried mines. The 'Generic Ocean Array Technology Sonar' (GOATS) trials in 1998 were the result of collaboration between Massachusetts Institute of Technology and the NATO Undersea Research Centre at La Spezia, Italy. The GOATS trials were intended to lay the groundwork for an MCM concept in which a single master vehicle and a network of AUVs worked together to detect and classify seabed targets in shallow water. In the actual experiment, carried out at the Isle of Elba, a single stationary parametric source was mounted on a tower rising 10m above the seabed. The secondary frequency band was 2-16 kHz. The receiver comprised an eight-element array mounted onto the front end of an Odyssey II AUV ('swordfish' configuration). The target field included three air-filled spherical steel shells and two water-filled steel cylinders. All these targets were partially or completely buried. The group subsequently published papers on the target imaging technique used [2], detection of buried mines [3] and the scope for subcritical insonification of the buried targets [4]. The group demonstrated bistatic synthetic aperture imaging of the buried target despite difficulties in synchronizing the transmitter and receiver records. Reflections from a second target lying proud of the surface provided the necessary reference point to link the records and focus the image.

Pinto [5] used the same transmitter as for the GOATS trials but his receiver was a static horizontal line array of length 12 m. He presents convincing images of proud and buried targets. The buried spherical target returns a series of echoes at characteristic times due to radiation by the various different wave types that are excited on its surface.

The Applied Research Laboratory at the University of Texas (Austin) has also reported preliminary results of a study of high-frequency bistatic synthetic aperture imaging [6]. ARL:UT uses a rotating turntable system at Lake Travis for sonar measurements.

In this paper we discuss the physical constraints that limit the motion of the transmitter and receiver of a bistatic synthetic aperture sonar system. The mathematical treatment parallels that given for bistatic SAR by Zeng, Cherniakov & Long [7] and Waltershied, Brenner & Ender [8]. The significant difference here is that the sonar receiver is a linear array of hydrophones, and this has implications for the allowable motion of both the transmitter and the receiver.

2.0 IMAGE OF A POINT TARGET

2.1 Matched filter response

We seek an expression for the image generated by the bistatic synthetic aperture sonar for a point target. We will see that this image is marred by grating lobes unless certain constraints on the motion of the transmitter and receiver are satisfied.

In line with normal sonar practice, the origin of Cartesian co-ordinates is at the sea surface. Depth is given by co-ordinate z. Initially we consider a single hydrophone. The geometry is shown in Figure 1. A point scatterer is located at $\mathbf{r}$. Both the transmitter and receiver travel in straight lines at constant speed in the directions given by (constant) unit vectors $\mathbf{d_1}$ and $\mathbf{d_2}$ respectively. u_1 and u_2 are the distances (m) covered by the transmitter and receiver respectively since they left their initial starting points. Both u_1 and u_2 are functions of a 'slow time' parameter ζ.

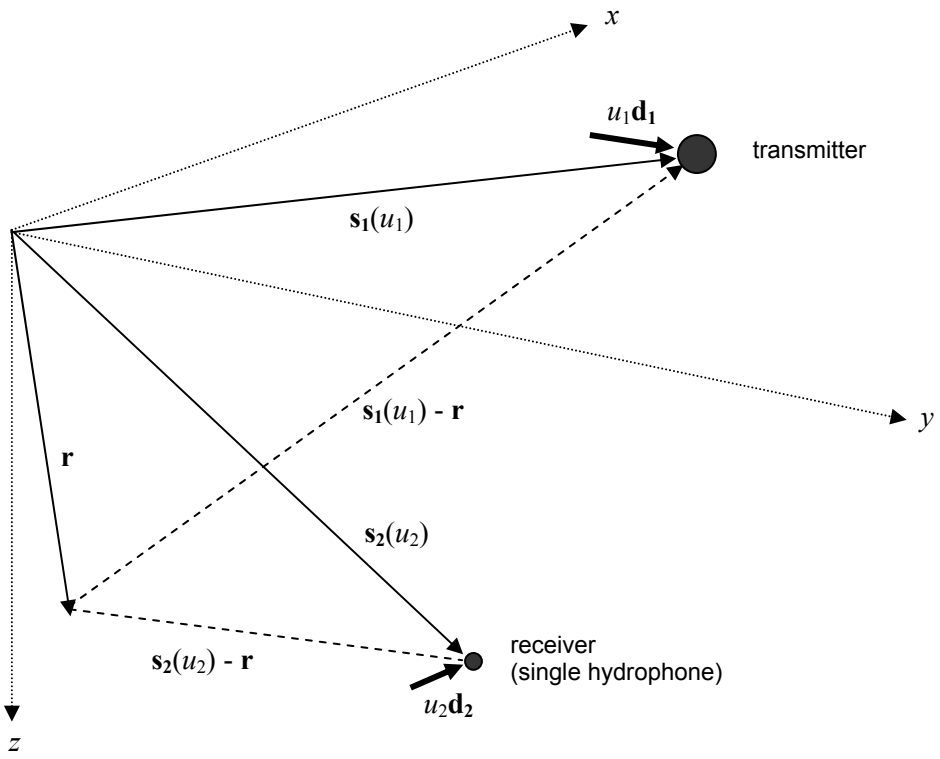

Figure 1: Geometry of bistatic SAS system (single hydrophone)

The distance from the transmitter to a scatterer at **r** is defined to be R_1, given by:

$$R_1 = \left|\mathbf{s}_1(u_1) - \mathbf{r}\right|$$

Similarly the distance from the scatterer to the receiver is:

$$R_2 = \left|\mathbf{s}_2(u_2) - \mathbf{r}\right|$$

For an arbitrary point **r'** close to **r**, we define:

$$R_1' = \left|\mathbf{s}_1(u_1) - \mathbf{r}'\right|$$
$$R_2' = \left|\mathbf{s}_2(u_2) - \mathbf{r}'\right|$$

The transmitter puts out a succession of modulated wideband chirp pulses that can be expressed in complex form as $p(t)\exp(j\omega_0 t)$ in which ω_0 is the carrier frequency (rad/s). The pulses received by the hydrophone are delayed versions of the transmitted pulse and for soundspeed c may be described by:

$$f(t,\zeta) = p\left(t - \frac{R_1 + R_2}{c}\right)\exp\left(j\omega_0\left(t - \frac{R_1 + R_2}{c}\right)\right)$$

(Note that R_1 and R_2 are functions of u_1 and u_2, which in turn depend on slow time parameter ζ.) The matched filter $h(t)$ for the given chirp signal is [9]:

$$h(t) = p^*(-t)\exp(j\omega_0 t)$$

The convolution of the received signal with the matched filter defines the *range* response of the point scatterer on the sonar image. For our purposes it is convenient to express the result in terms of a range variable rather than time. In a change of variables, we replace t by the corresponding total distance via an arbitrary point:

$$t \to \frac{R_1' + R_2'}{c}$$

We may then convolve the received signal with its matched filter to obtain a result that is similar in form to that of [10]. t is reintroduced as a dummy variable of integration.

$$g(R_1' + R_2', \zeta) = \exp\left(j\frac{\omega_0}{c}(R_1' - R_1 + R_2' - R_2)\right)\int_{-\infty}^{\infty} p^*\left(t - \frac{R_1' + R_2'}{c}\right)p\left(t - \frac{R_1 + R_2}{c}\right)dt$$

The complete response of the synthetic aperture system to a scatterer at **r** is obtained by summing the response $g(R_1' + R_2', \zeta)$ over all pings. This result has been termed the generalised ambiguity function, Φ [8,10].

$$\Phi(\mathbf{r}';\mathbf{r}) = \sum_{pings}\exp\left(j\frac{\omega_0}{c}(R_1' - R_1 + R_2' - R_2)\right)\int_{-\infty}^{\infty} p^*\left(t - \frac{R_1' + R_2'}{c}\right)p\left(t - \frac{R_1 + R_2}{c}\right)dt$$

In synthetic aperture sonar calculations it is normally assumed that R_1 and R_2 do not change significantly over the course of the matched filter calculation – the 'stop-start assumption' (although in practice it is necessary to take account of motions that take place while the sound pulses are in transit). Therefore, the integration over time can be considered separately from the summation over pings, and we may write

$$\Phi(\mathbf{r}';\mathbf{r}) = \Phi_{dd}(\mathbf{r}';\mathbf{r})\Phi_{pp}(\mathbf{r}';\mathbf{r})$$

The integration over time gives rise to Φ_{pp}, a sinc function in range, while the summation of exponential phase terms over M pings gives rise to Φ_{dd}, a grating function of the form $\sin(M\phi)/\sin\phi$. In monostatic SAS these two terms appear perpendicular to each other (across-track and along-track, *i.e.* range and azimuth). In bistatic SAS they are not perpendicular in general. In the following sections we discuss each of these two terms in more detail.

2.2 Sinc function in range

The sinc function in range is the evaluation of the integral:

$$\Phi_{pp}(\mathbf{r}';\mathbf{r}) = \int_{-\infty}^{\infty} p^*\left(t - \frac{R_1' + R_2'}{c}\right) p\left(t - \frac{R_1 + R_2}{c}\right) dt$$

Taking $p(t)$ to be a chirp function of bandwidth B (Hz), the above integral can be simplified using Parseval's theorem to give:

$$\Phi_{pp}(\mathbf{r}';\mathbf{r}) = \int_{-B/2}^{B/2} \exp\left(j2\pi f \frac{R_1' - R_1 + R_2' - R_2}{c}\right) df$$

The sinc function Φ_{pp} will clearly peak when $\mathbf{r}' = \mathbf{r}$, *i.e.* when $R_1' = R_1$ and $R_2' = R_2$. However, we need to know the alignment of the sinc function, seen when the trial point $\mathbf{r}'$ is *near* to $\mathbf{r}$.

We note that $R_1(\mathbf{r})$ is a scalar field. A little algebra shows that its *gradient* is given by:

$$\nabla R_1 = -\frac{\mathbf{s}_1(u_1) - \mathbf{r}}{R_1}$$

Similarly

$$\nabla R_2 = -\frac{\mathbf{s}_2(u_2) - \mathbf{r}}{R_2}$$

When the observation point $\mathbf{r}'$ is close to the scatterer $\mathbf{r}$, we may write the difference $(R_1' - R_1)$ approximately in the form of a dot product:

$$R_1' - R_1 \approx (\mathbf{r}' - \mathbf{r}) \bullet \nabla R_1$$

and similarly for $(R_2' - R_2)$. Substituting for $(R_1' - R_1)$ and $(R_2' - R_2)$ and evaluating the integral, we obtain the sinc function in range as:

$$\Phi_{pp}(r'; r) = B \operatorname{sinc}\left(\frac{B}{c} (\mathbf{r}' - \mathbf{r}) \bullet (\nabla R_1 + \nabla R_2) \right)$$

Figure 2 shows the geometry of the situation, projected onto a plane (*e.g.*, a flat seabed, z = constant) for imaging. Note that the gradient vectors have unit length in three-dimensional space but may be shorter when projected onto a plane surface.

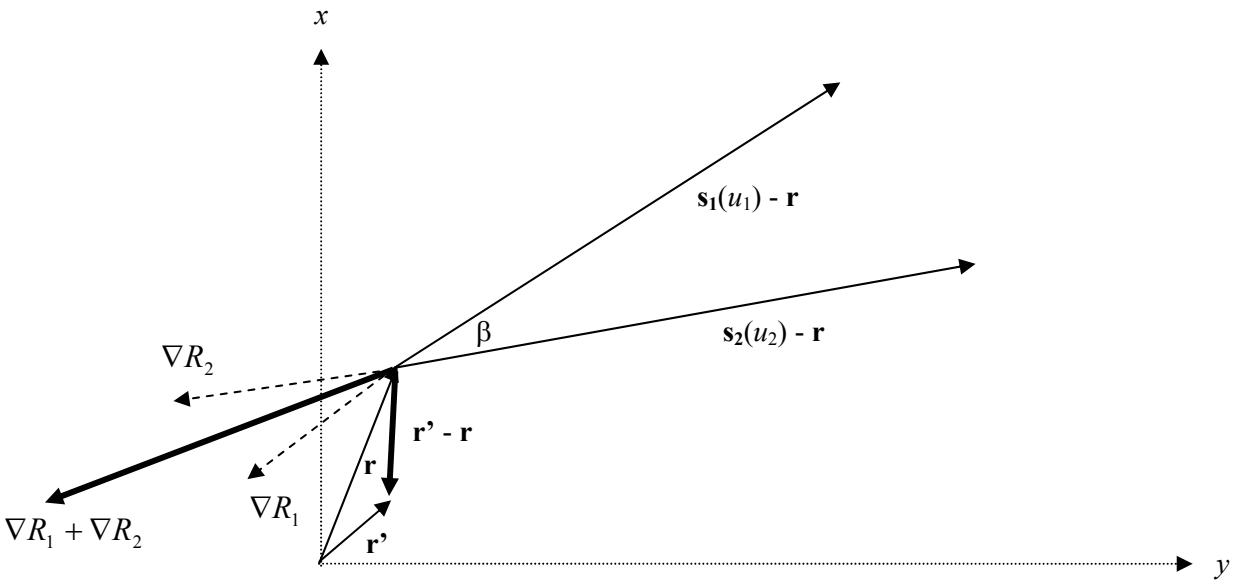

Figure 2: Geometry of range resolution of bistatic sonar system. There is a point scatterer at r. The image is evaluated in terms of r' on a plane of constant depth. The peak of the sinc function extends along a line perpendicular to the sum of the gradient vectors.

The finest resolution occurs in the direction of the sum of gradients. If the transmitter, receiver and scatterer are coplanar, the gradient vectors are both unit vectors and the sum of gradients always occurs at the bisector of the bistatic angle β.

2.3 Sum over pings

The sum over pings Φ_{dd} in the generalised ambiguity function is given by:

$$\Phi_{dd}(\mathbf{r}';\mathbf{r}) = \sum_{pings} \exp\left(j\frac{2\pi}{\lambda}(R_1'-R_1 + R_2'-R_2) \right)$$

in which λ is the wavelength of the carrier frequency. We wish to put this into the following more convenient form in which wavenumbers appear. The wavenumbers will determine the form and direction of the grating function in azimuth.

$$\Phi_{dd} = \sum_{pings} \exp(jk_{u1}u_1)\exp(jk_{u2}u_2)$$

The wavenumber k_{u1} is given by:

$$k_{u1} = \frac{\partial}{\partial u_1}\left[\frac{2\pi}{\lambda}(R_1'-R_1)\right] = \frac{\partial}{\partial u_1}\left[\frac{2\pi}{\lambda}(\mathbf{r}'-\mathbf{r})\bullet\nabla R_1\right] = \frac{2\pi}{\lambda}(\mathbf{r}'-\mathbf{r})\bullet\frac{\partial}{\partial u_1}(\nabla R_1)$$

and k_{u2} has the corresponding form with u_2, R_2' and R_2. Expressing the vectors in terms of their Cartesian co-ordinates and use of a little algebra shows that:

$$\frac{\partial}{\partial u_1}(\nabla R_1) = -\frac{1}{R_1}\left[\mathbf{I} - \frac{(\mathbf{s}_1(u_1)-\mathbf{r})(\mathbf{s}_1(u_1)-\mathbf{r})^T}{R_1^2}\right]\mathbf{d}_1$$

Here, **I** is the 3x3 unit matrix. The term in square brackets is a projection array, which we will designate $\mathbf{P}_1(u_1; \mathbf{r})$ from now on. It has the effect of projecting the unit vector $\mathbf{d}_1$ (which indicates the direction of motion of the transmitter) onto the perpendicular to the vector in the direction of the scatterer, $\mathbf{s}_1(u_1) - \mathbf{r}$, as shown in Figure 3. A similar projection array $\mathbf{P}_2(u_2; \mathbf{r})$ arises for the receiver.

Using these results, the wavenumbers become:

$$k_{u1} = -\frac{2\pi}{\lambda}(\mathbf{r}'-\mathbf{r})^T\frac{\mathbf{P}_1(u_1;\mathbf{r})\mathbf{d}_1}{R_1}$$

$$k_{u2} = -\frac{2\pi}{\lambda}(\mathbf{r}'-\mathbf{r})^T\frac{\mathbf{P}_2(u_2;\mathbf{r})\mathbf{d}_2}{R_2}$$

Having now evaluated k_{u1} and k_{u2}, we are in a position to carry out the summation for $\Phi_{dd}(\mathbf{r}'; \mathbf{r})$.

2.4 Receiver hydrophone array

Thus far, u_1 and u_2 have expressed the distance travelled by a point transmitter and point receiver respectively. We now specify more detail for the transmitter and receiver motions and introduce an *array* of hydrophones as the receiver.

Let the distance travelled by the transmitter from one ping to the next be Δ_1, and the distance travelled by the receiver from one ping to the next, Δ_2. Furthermore, let the receiver consist of an array of N

hydrophones separated by a distance δ. The hydrophones are lined up in the direction of travel, $\mathbf{d}_2$. Taking the number of pings as M, we have

$$u_1 = m\Delta_1$$
$$u_2 = m\Delta_2 + n\delta \qquad m = 0,1,2,...M-1; \qquad n = 0,1,2...N-1$$

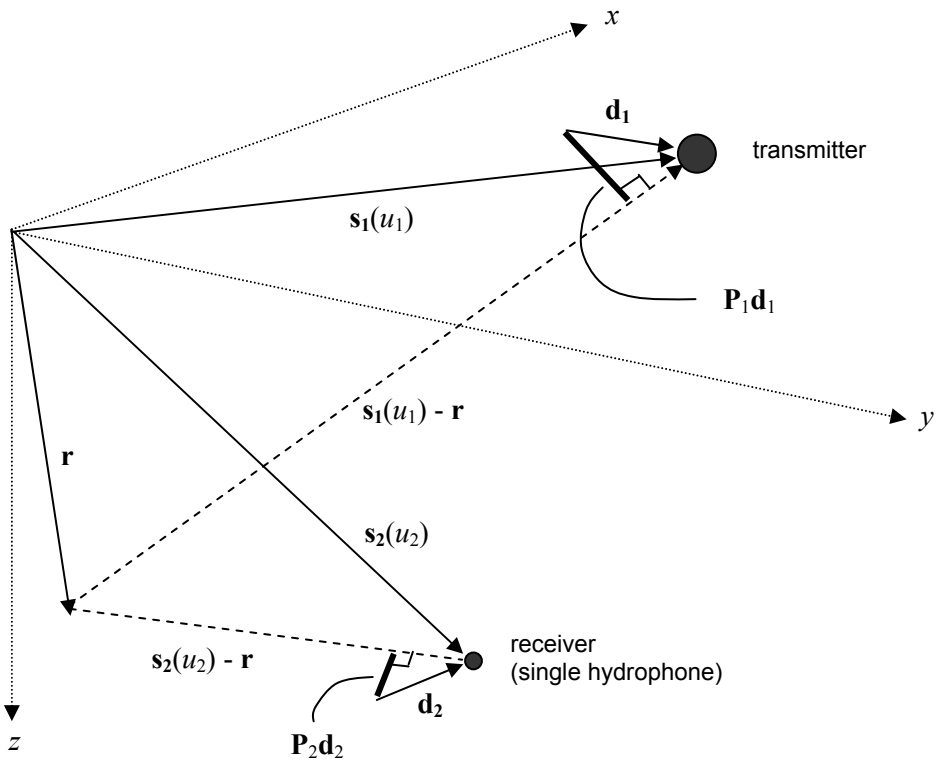

Figure 3: Projection of transmitter and receiver direction vectors. The vectors P_1d_1 and P_2d_2 are perpendicular to the respective vectors joining the transmitter (or receiver) and the point scatterer at r.

The expression for Φ_{dd} becomes a double summation over m and n:

$$\Phi_{dd}(\mathbf{r}';\mathbf{r}) = \sum_{m=0}^{M-1}\sum_{n=0}^{N-1}\exp(jk_{u1}m\Delta_1)\exp(jk_{u2}(m\Delta_2 + n\delta))$$
$$= \sum_{m=0}^{M-1}\exp(jm(k_{u1}\Delta_1 + k_{u2}\Delta_2))\sum_{n=0}^{N-1}\exp(jk_{u2}n\delta)$$

Evaluating the summations leads to a product of grating functions of the form $\sin(M\phi)/\sin\phi$ (see Figure 4).

$$\Phi_{dd}(\mathbf{r}';\mathbf{r}) = A\frac{\sin\left[M\dfrac{(k_{u1}\Delta_1 + k_{u2}\Delta_2)}{2}\right]}{\sin\left(\dfrac{k_{u1}\Delta_1 + k_{u2}\Delta_2}{2}\right)}\frac{\sin\left(N\dfrac{k_{u2}\delta}{2}\right)}{\sin\left(\dfrac{k_{u2}\delta}{2}\right)}$$

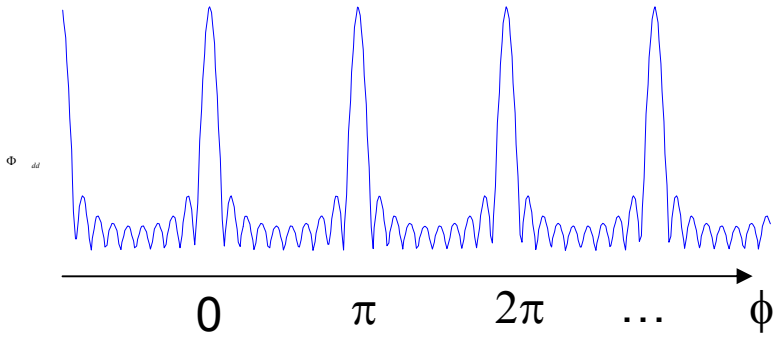

Figure 4: Form of grating function sin(Mϕ)/sinϕ for M=10. (Absolute value)

If the hydrophone spacing δ and the motion per ping Δ_2 are chosen arbitrarily, grating lobes appear at intervals when $(k_{u1}\Delta_1 + k_{u2}\Delta_2) = 2\pi$. In a monostatic system, this interval would correspond to disruptions once per ping in the line of phase centres of the synthetic array. The result would be a set of 'ghost' images of the point target, familiar as grating lobes on the synthetic aperture image. On the other hand, if the directions and intervals are chosen correctly, the denominator of the first term of Φ_{dd} will cancel with the numerator of the second term. In this case the grating lobes will be occur at intervals corresponding to $k_{u2}\delta = 2\pi$. As the hydrophone spacing δ is small, the grating lobes will be very widely spaced. This second case corresponds in a monostatic system to a synthetic aperture that comprises a continuous line of phase centres.

The condition for no grating lobes is thus:

$$k_{u1}\Delta_1 + k_{u2}\Delta_2 = k_{u2}N\delta$$

For example, in the monostatic case, $\Delta_1 = \Delta_2 = \Delta$, $k_{u1} = k_{u2} = k_u$ and the condition becomes:

$$\Delta = \frac{N\delta}{2}$$

Thus the hydrophone array should travel exactly half its own length between pings, as expected for monostatic synthetic aperture sonar. For the bistatic case we write in the full expressions for k_{u1} and k_{u2} to obtain:

$$(\mathbf{r}'-\mathbf{r})^T\left(\frac{\mathbf{P}_1\mathbf{d}_1}{R_1}\Delta_1 + \frac{\mathbf{P}_2\mathbf{d}_2}{R_2}\Delta_2\right) = (\mathbf{r}'-\mathbf{r})^T\frac{\mathbf{P}_2\mathbf{d}_2}{R_2}N\delta$$

We require this expression to be satisfied for all points **r'** in the vicinity of the scatterer at **r** in order to form an image. In general, however, the vector $\mathbf{P}_1\mathbf{d}_1$ points in a different direction from $\mathbf{P}_2\mathbf{d}_2$ (see Figure 3). It is clear by inspection that the condition cannot be satisfied unless $\mathbf{P}_1\mathbf{d}_1$ either points in the same direction as $\mathbf{P}_2\mathbf{d}_2$ or (alternatively) $\Delta_1 = 0$.

If $\mathbf{P}_1\mathbf{d}_1$ points in the same direction as $\mathbf{P}_2\mathbf{d}_2$, this would imply that the transmitter and receiver view the point scatterer along the same line (though not necessarily from the same distance). If they view along the same line and *are* at the same distance, the system is monostatic.

On the other hand, if $\Delta_1 = 0$ this would imply that the transmitter is stationary. In this case the constraint reduces to:

$$\Delta = N\delta$$

Thus bistatic synthetic aperture imaging is possible provided the transmitter is essentially stationary during the formation of the synthetic aperture. An image free of grating lobes can be formed if the receiver array moves its own entire length ($N\delta$) from one ping to the next – double the speed allowed for monostatic SAS.

3.0 CONCLUSION

The paper has set out the constraints on the motion of the transmitter and the receiver hydrophone array if the returning signal from the target area is to be adequately spatially sampled. In particular, it is shown that the movement of the transmitter is severely constrained if a chosen target area is to be sampled without grating lobes. The transmitter must either be stationary or must move in such a way that its line of sight to the target area is the same as that of the receiver array while the synthetic aperture is being formed. (The transmitter need not be the same distance away as the receiver, however, and it need not travel in the same direction.)

If the transmitter is stationary, the receiver array can move its entire length between pings as opposed to half its length as in the case of monostatic SAS.

These constraints do not arise in bistatic synthetic aperture radar, where the receiver is a single antenna, not a linear array.

4.0 REFERENCES

[1] G Yates (2005) *Bistatic Synthetic Aperture Sonar*. PhD Thesis, University of London, 2005.

[2] J R Edwards, H Schmidt and Kevin LePage (2001). *IEEE J Oceanic Engng.* **26**(4) Oct 2001 pp 690-699. Bistatic Synthetic Aperture Target Detection and Imaging with an AUV.

[3] Kevin D LePage and Henrik Schmidt (2002). *IEEE J Oceanic Engng*. **27**(3) July 2002 pp 471-483. Bistatic Synthetic Aperture Imaging of Proud and Buried Targets from an AUV.

[4] I Veljkovic, J R Edwards and H Schmidt (2001). *Proc OCEANS 2001*, 5-8 Nov 2001 Vol 1 pp 59-62. Sub-critical Insonification of Buried Elastic Targets.

[5] M A Pinto, A Bellettini, R Hollett and A Tesei (2002). *IEEE J Oceanic Engng.* **27**(3) July 2002.pp 484-494. Real- and Synthetic-Array Processing of Buried Targets.

[6] S K Mitchell (2004) *6th Int Symp on Technology and the Mine Problem,* Monterey CA 9-13 May 2004. High Resolution Bistatic and Monostatic Circular SAS Imaging at Search Frequencies.

[7] T Zeng, M Cherniakov and T Long (2005) *IEEE Trans Aerospace & Electronic Systems* **41**(2) April 2005 pp 461-474. Generalized approach to resolution analysis in BSAR.

[8] I Waltershied, A R Brenner and J H G Ender (2004) *Proc EUSAR 2004* pp 567-570. Geometry and System Aspects for a Bistatic Airborne SAR-Experiment.

[9] M Soumekh (1999) *Synthetic Aperture Radar Signal Processing*. John Wiley & Sons, 1999.

[10] M Skolnik (1990) Radar Handbook 2nd Edition (Chapter 21 – Synthetic Aperture Radar, by L J Cutrona). Mc Graw Hill, 1990.